J. Mol. Model. **2000**, *6*, 26 – 34

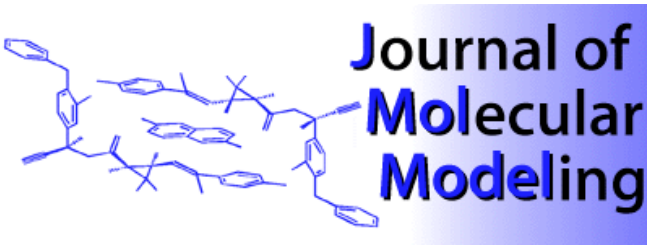

FULL PAPER

Be^{2+} V^{-} Dipole and Adsorptivity of Atomic H on LiH(001) Surface: ab initio Study

Ahmed S. Shalabi[1], Ahmed M. El-Nahas[2], and Amany A. Shalabi[2]

[1]Department of Chemistry, Faculty of Science, Benha University, Benha, Egypt. Fax: +20-2-4188738.
E-mail: a.m.elmahdy@mailcity.com

[2]Department of Chemistry, Faculty of Science, El-Menoufia University, Shebin El-Kom, Egypt

Received: 25 May 1999/ Accepted: 18 November 1999/ Published: 4 February 2000

Abstract An attempt has been made to examine the properties of the title divalent cation impurity - cation vacancy dipole as well as the adsorptivity and diffusion of atomic hydrogen over the LiH (001) surface using *ab initio* methods of molecular electronic structure calculations. The LiH crystal surface was simulated and quantum clusters of variable size were surrounded by point charges to examine the I-V dipole orientation, cation vacancy migration and overlap effects. The effects of introducing an I-V dipole on the nature of adsorbate-substrate interactions and diffusion of an H atom over the surface were also examined. The results confirm that the (100) orientation of the I-V dipole is energetically more favorable than the (110) orientation and that the cation vacancy migrates without activation energy barriers. The I-V dipole enhances the adsorptivity of atomic hydrogen by ca. 4.96 eV, changes the nature of adsorption from physisorption to chemisorption and introduces an activation energy barrier to H diffusion over the surface. As the I-V dipole is introduced, the HOMO and LUMO levels of the substrate shift to higher energies, the band gap becomes narrower and the atomic charges on the adsorbed H increases. This change in the electronic structure makes the adsorptivity process, through the charge transfer from the H 1s singly occupied AO to the conduction band and from the valence band to the H 1s singly occupied AO more facile.

Keywords I-V dipoles, Surface adsorption, Band gaps, LiH crystal, ab initio

Introduction

Ab initio methods are being used increasingly to probe the properties of condensed matter. Of particular importance is the behavior of defects or impurities, which control the mechanical properties of crystalline solids. Divalent cation impurities constitute the major contamination in ionic crystals. They lie at a substitutional position and present an excess positive charge. This in turn induces the generation of a cation vacancy to retain the electrical neutrality of the material.

Because of the Coulomb attraction, the energetically most favored location for the vacancy is as nearest or next nearest neighbors to the impurity. In each case, an impurity - vacancy (I-V) dipole is created with orientation (100) for nearest neighbors and (110) for next nearest neighbor dipoles.

Correspondence to: A. S. Shalabi

Direct evidence for the occurrence of both types of dipoles has been obtained from electron spin resonance (ESR) spectra of transition - metal ion (Mn^{2+}) and rare earth ion (Eu^{2+}) [1].

The I-V dipole is thermally dissociated and free dissociation energies and vacancy migration energies can be obtained from ionic conductivity measurements. Thermal orientation of these dipoles can be studied from the electric losses or by using the ionic thermocurrent method developed by Bucci and Fieschi [2].

Detailed experimental studies have been carried out on a number of divalent cations. Optical spectroscopy has been applied to Pb^{2+} and Sn^{2+} and optical and magnetic ESR and ENDOR spectroscopy to transition metals (e.g. Mn^{2+} and Ni^{2+}) and rare earth ions (e.g. Eu^{2+}) and the experimental data have been generally analyzed in accordance with the conventional schemes of the crystal and ligand field methods [3,4]. Varostos and Mourikis [5] calculated the association energy of the Mg^{2+} - cation vacancy in LiD and LiH from conductivity measurements. Ikeya [6] calculated the energy of association of a positive ion vacancy with a divalent cation impurity in LiH from the ionic conductivity measurements as well as the energy of the rotation of a vacancy around cation from the measurements of ionic thermocurrent (ITC). Kalman et al. [7] using computed ionic displacements and elastic stress field of dislocations calculated the yield stress increment caused by I-V dipoles in NaCl crystal containing Ca^{2+} impurities. Toth et al. [8] computed the interaction of dislocations with both fixed and rotating I-V dipoles with edge and screw dislocation.

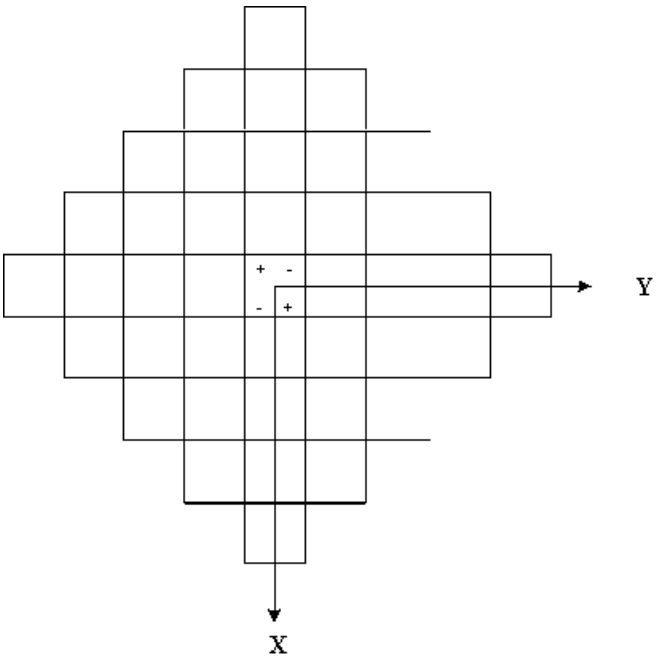

Figure 1 *Representation of the z = 0 plane of the lattice used in the calculations*

Table 1 *Specification of the finite lattice used for the crystal calculations. R is half the lattice distance which for LiH is 2.04Å; r is the distance of the appropriate shell from the center of the lattice*

r^2/R^2	Coordinates/R |X|, |Y|, -Z	Charge |q|	Number of centers
2	1 1 0	1	4
6	1 1 2	1	4
10	3 1 0	1	8
14	3 1 2	1	8
18	1 1 4	1	4
18	3 3 0	1	4
22	3 3 2	1	4
26	5 1 0	1	8
26	3 1 4	1	8
30	5 1 2	1	8
34	3 3 4	1	4
34	5 3 0	1	8
38	5 3 2	1	8
38	1 1 6	1	4
42	5 1 4	1	8
46	3 1 6	1	8
50	5 5 0	1	4
50	5 3 4	1	8
50	7 1 0	1	8
54	5 5 2	1	4
54	3 3 6	1	4
58	7 3 0	1	8
66	5 5 4	1	4
54	7 1 2	0.409283	8
62	7 3 2	0.409283	8
66	1 1 8	0.800909	4
82	9 1 0	0.800909	8
86	9 1 2	0.800909	8

Theoretical and experimental studies of adsorption on solid surfaces have become of increasing importance [9]. This is attributed to the fact that they are related to a variety of technologically significant processes, not least of which are catalysts, corrosion and gas sensors. The chief problem in studying these processes computationally is the treatment of the extended surface when examining a localized phenomenon like chemisorption [10]. For simple systems such as atoms or small molecules interacting on surfaces, it can be feasible to use an extended 2- dimensional periodic system and to study an ordered overlayer of adsorbate on the surface. Such examinations have sometimes used slab calculations [11], although more recently surface embedding is providing a promising route forward. Several theoretical studies have been done to simulate adsorption of simple systems on ionic surfaces [12-15]. For oxide surfaces, these studies highlight the formation of metal-oxygen bonding and antibonding states, the later being either completely or partially filled. Thus the interactions are considered to be mainly of a chemical nature.

This is a reasonable assumption for relatively reactive surfaces such as those of many metal oxides. However, other ionic surfaces are known to be highly stable and the nature of the metal-surface (100) bond is not so clear. Meanwhile, we have not been able to find any experimental data on the characteristics of hydrogen adatoms on lithium-hydride surfaces, hence our results serve as theoretical predictions.

Methods

In cluster calculations, the host surface is represented by only a small number of ions explicitly in the three dimensional space. The remainder may be represented by some long range potential, like Madelung potential, or may be merely ignored. To simulate the LiH crystal surface, we follow a procedure previously reported for MgO crystals [16]. A finite crystal of 288 point charges was first constructed. The Coulomb potential along the *x*- and *y*-axes of this crystal are zero by symmetry as in the host crystal, Figure 1. The charges on the outer shells listed in Table 1 were modified to make the Coulomb potential at the four central sites equal to the Madelung potential of the host crystal and to make the eight points with coordinates (0, ± R, ± R) and (± R, 0, ± R), where R is half the lattice distance which for LiH is 2.04 Å, equal to zero as it should be in the host crystal. With these charges, 0.409283 and 0.800909, the Coulomb potential in the region occupied by the central ions is very close to that in the unit cell of the host crystal. All charged centers with cartesian coordinates ±X, ±Y and Z=2R, 4R, 6R and 8R were then removed, so that the surface generated consists of 176 charged centers in the three dimensional space ±X, ±Y and -Z = 0,2R, 4R, 6R and 8R. The coordinates of these charged centers are given in Table 1. Ion clusters were then embedded within the central region of the crystal surface to examine the required properties. All the electrons of the embedded clusters were included in the Hamiltonian of *ab initio* calculations. Other crystal sites entered the Hamiltonian of *ab initio* calculations as point charges. The adsorbate-substrate distances were then optimized and gas-surface potentials were calculated.

In order to understand the possible electrostatic contribution to the bonding when using Li_2H_2, Li_8H_8 and $Li_{14}H_{14}$ clusters, plus corresponding embedding for the surface, we calculated the electrostatic potential at the surface on the (0,0,0) site for each cluster. Figure 2 shows that the electrostatic potentials due to Li_8H_8 and $Li_{14}H_{14}$ are slightly different and the shapes of functions are quite similar. This means that we can expect almost the same electric fields and electric field derivatives. Since the electrostatic interaction of the adatom with the surface will mainly consist of electric field-induced dipole and electric field derivatives-induced quadruple moments, one expects that the classical contributions to the adatom-surface interactions are quite similar for clusters with sizes larger than those considered in the present study.

The Hartree-Fock method of *ab initio* theory employed in the present calculations treats the exchange potential exactly, but omits - by definition - the correlation energy. Since cor-

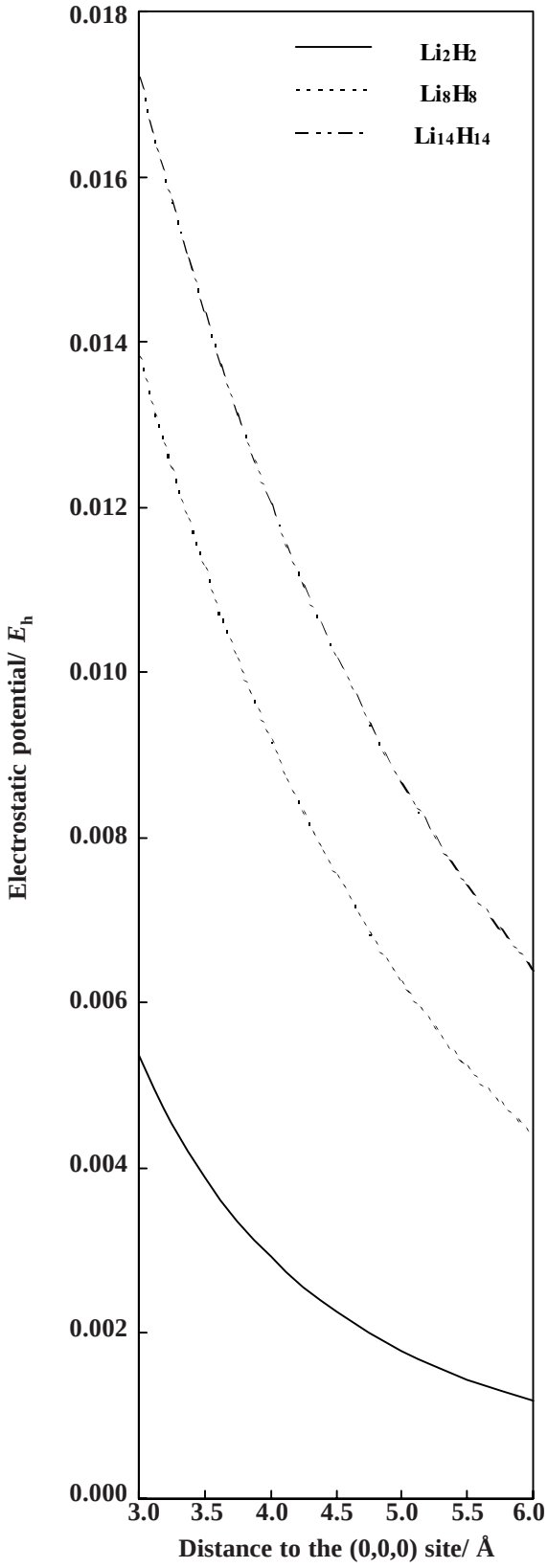

Figure 2 *Electrostatic potentials as a function in the distance to the 0,0,0 site of Li_2H_2, Li_8H_8 and $Li_{14}H_{14}$ clusters*

Table 2 *Binding energies of the (110) and (100) orientations of I-V dipole using SCF and DFT methods and different cluster sizes: BeH_2, $BeLi_6H_8$ and $BeLi_{12}H_{14}$. Energies are given in eV*

		BeH_2	$BeLi_6H_8$	$BeLi_{12}H_{14}$
(110)	SCF	-1.897	1.420	8.424
	DFT	-2.509	-0.677	5.360
(100)	SCF	-5.534	-1.234	5.452
	DFT	-6.586	-4.070	1.865

relation energy is mainly responsible for the attractive van der Waals interactions between adsorbates and substrate surfaces, the influence of Density Functional Theory DFT correlation at the B3LYP level and 6-31++G (d, p) basis sets has been tested for (110) and (100) orientations of the I-V dipole using BeH_2, $BeLi_6H_8$ and $BeLi_{12}H_{14}$ clusters. In Table 2, the binding energies of the two IV orientations at different cluster sizes are given. As shown in this Table, the contribution of the DFT correlation ranges from ca. 0.5442 to 2.9931 eV for the (110) orientation and from ca. 1.0884 to 2.9931 eV for the (100) orientation. However, for the more stable (100) orientation, the contributions to $BeLi_6H_8$ and $BeLi_{12}H_{14}$ clusters are nearly identical (ca. 2.9931 eV).

The Hartree-Fock calculations were carried out using the Gaussian 6-31++G(d,p) internal basis. For an ionic cluster such as Li_8H_8 on which atomic H is adsorbed, there are 206 basis functions and 328 primitive Gaussians. As shown the basis set size is large enough to minimize the basis set superposition error BSSE. The basis set superposition errors for a sample of 4 ions cluster (Li_2H_2) were calculated to be ca. -0.0010, -0.0015 and –0.0015 E_h using the basis sets 6-31++G (d, p), 6-311++G (d, p) and 6-31++G (2df, 2pd) respectively. Moreover, since the most important nearest neighbor ions to the four central sites are included explicitly in the calculations, the accuracy of the results might be significantly affected by including the relatively less important long range potentials of next nearest neighbors. The quantum mechanical calculations were carried out using Gaussian98 system [17].

Results and discussion

$Be^{2+}V^{-}$ dipole orientation

We first examine the preferred orientation of $Be^{2+}V^{-}$ dipole at the surface of the crystal. Two- possible orientations are considered (110) and (110). These are shown in Figure 3. For each orientation, two- ion clusters of variable size are investigated, BeH_2 and $BeLi_6H_8$. The first represents three interacting ions and a cation vacancy. The second is identical to the first, but surrounded by 6 Li^+ and 6H^- ions representing the nearest neighbors to the four central sites. In other words, the nearest neighbor point charges to the BeH_2 cluster were replaced by real ions to examine the overlap effects on interaction energies. The non-Coulombic interaction energy (binding energy) of each ion cluster was calculated by subtracting the non-Coulombic monomer energies from the non-Coulombic total energies. The non-Coulombic interaction energies of (110) orientation were calculated to be ca. -1.9 eV for BeH_2 and ca. 1.42 eV for $BeLi_6H_8$.

The non-Coulombic interaction energy of the (100) orientation was calculated to be ca. -5.53 eV for BeH_2 and ca. -1.77 eV for $BeLi_6H_8$. On this basis, the (100) orientation is suggested to be the more energetically preferred orientation of $Be^{2+}V^{-}$ dipole at the surface of the crystal. The non-Coulombic interaction energy implies that binding energy is calculated in the absence of the point charge distribution. Consequently - in the absence of such stabilizing long range fields - the clusters can be unstable. This is indicated by the previous less negative values of binding energies for $BeLi_6H_8$ cluster in the (100) and (110) orientations.

To have an estimate of the electron correlation effects, we carried out DFT calculations on the binding energies of (100)

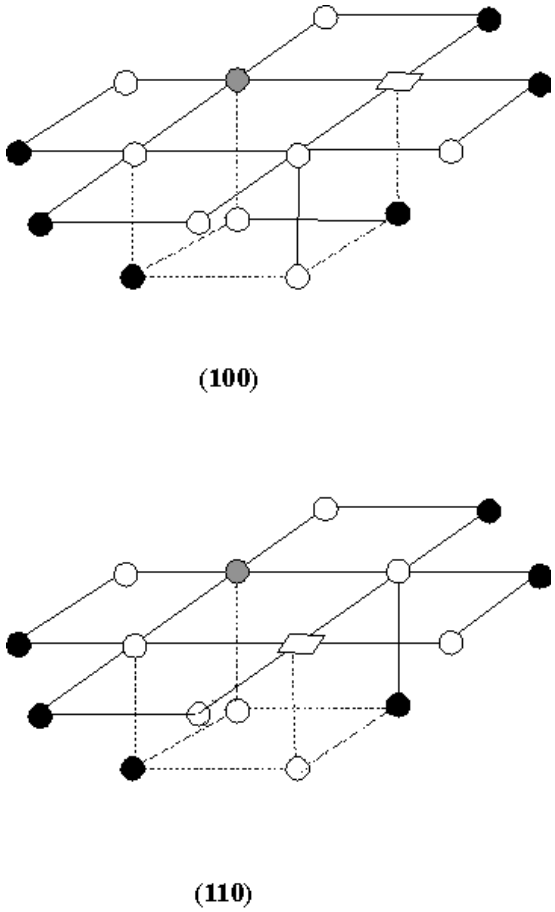

Figure 3 *(110) and (100) orientations of $Be^{2+}V^{-}$ dipole at the surface of LiH. ●: Be^{2+}, ○: H^-; ●: Li^+; □: vacancy*

Table 3 *The data for the selected substrate locations Δ, equilibrium adsorption energies $E_{ads.}$/eV and atom-surface distances Re/Å of atomic H over the defect-free (Li_2H_2 and Li_8H_8) and defect-containing (BeH_2 and $BeLi_6H_8$) surfaces of LiH*

	Li_2H_2		Li_8H_8	
Δ	**Re**	**Eads.**	**Re**	**Eads.**
0.0	4.50	-0.00254	4.00	-0.00803
0.1	4.60	-0.00252	3.90	-0.00889
0.2	4.75	-0.00249	3.75	-0.00969
0.3	4.75	-0.00245	3.80	-0.01002
0.4	4.75	-0.00240	3.80	-0.01011
0.5	4.70	-0.00236	3.80	-0.00993
0.6	4.70	-0.00231	3.60	-0.00973
0.7	4.60	-0.00227	3.60	-0.00920
0.8	4.50	-0.00224	3.70	-0.00867
0.9	4.40	-0.00223	3.70	-0.00881
1.0	4.40	-0.00223	3.60	-0.00770
	BeH_2		$BeLi_6H_8$	
Δ	**Re**	**Eads.**	**Re**	**Eads.**
0.0	1.330	-4.0099	1.35	-4.0450
0.1	1.310	-4.2007	1.30	-4.2311
0.2	1.260	-4.3776	1.25	-4.3998
0.3	1.170	-4.5440	1.15	-4.5547
0.4	1.100	-4.6808	1.02	-4.7056
0.5	0.800	-4.8713	0.80	-4.8416
0.6	0.400	-5.0699	0.55	-4.9674
0.7	-0.035	-5.2279	0.20	-4.9663
0.8	-0.090	-5.0251	0.10	-4.6824
0.9	-0.150	-4.6655	0.10	-4.2451
1.0	-0.200	-4.2676	0.10	-3.7478

and (110) orientations of I-V dipoles for BeH_2, $BeLi_6H_8$ and $BeLi_{12}H_{14}$ clusters. The DFT results are collected with the SCF results - for comparison - in Table 2. As shown in this table, binding energies are quite sensitive to cluster size. The trend is that cluster stability is inversely proportional to cluster size, as indicated by the less negative or more positive values of binding energies. This is a logical consequence of the absence of the stabilizing effects of Coulombic interactions which are – as shown – directly proportional to cluster size. However, when we come to consider the relative stabilities of the two considered orientations, the (100) orientation was always more stable than the (110) at the SCF and DFT levels. The (100) orientation was energetically preferred by ca. 3 to 3.5 eV at the SCF level and by ca. 3.5 to 4.6 eV at the DFT level. Moreover, the contribution of DFT electron correlation is significant and ranges from 0.61 to 3.06 for (100) orientation, and from 1.05 to 3.59 for (110) orientation. The electron correlation contribution is also shown to be a function of cluster size, i.e., the DFT contribution is directly proportional to the size of the embedded cluster.

To shed light on the geometrical relaxation effects, we have considered the relaxation of nearest neighbor ions to the I-V dipole in the (100) orientation of $BeLi_3H_5$ embedded cluster. The optimal relaxation mode was found to be associated with the outward displacement of all nearest neighbor ions. Outward displacement by 10% of the interionic separation lowers the total energy by ca. 0.59 eV at the SCF level and ca. 0.56 eV at the DFT level.

The difference in binding energies between BeH_2 and $BeLi_6H_8$ ion clusters may be taken as a measure for the magnitude of overlap effects. These contribute ca. 3.32 eV to the total binding energy of the (110) orientation and ca. 3.76 eV to the total binding energy of the (100) orientation. In other words, they contribute ca. 0.72 eV to the total binding energy per ion of the (110) orientation and ca. 1.72 eV to the total binding energy per ion of the (100) orientation. These minor changes in binding energies with increasing cluster size should be mainly attributed to placing the ion clusters in the simulated Coulomb field of the host surface. On the other hand, the difference in binding energies of the two orientations may be taken as a measure for the energy required for cation vacancy migration between the two neighboring sites shown in Figure 3. These were calculated to be 3.63 eV for BeH_2 cluster and 3.19 eV for $BeLi_6H_8$ cluster pointing to the ease of cation vacancy migration between the two relevant sites, provided that no activation barriers exist. We have therefore examined the presence of activation barriers for the migration of cation vacancy by calculating the binding energies of BeH_2 and $BeLi_6H_6$ ion clusters as a function in the diffusion path Δ. The data are represented graphically in Figure 4. As shown in this figure, no activation barriers exist for the migration of the cation vacancy from the (110) orientation to

the (100) orientation in consistence with the prediction that the (100) orientation is the more energetically favorable orientation at the surface. The energy gaps between the two ion clusters along the diffusion path Δ reflect the contributions of overlap effects, relative to crystal field effects, and are shown to be significantly broadened at the preferred orientation (100).

Adsorptivity of atomic H

In general, adsorbate - substrate interactions result from the tendency of the adsorbate valence electrons to interact with the available substrate electronic states. This interaction can be expected to have a major role if there exists a small energy gap between the adsorbate and substrate electronic states, or if the adsorbate has an open shell electronic structure.

We discuss our results of adsorbate-substrate interactions by studying the diffusion characteristics of a single H atom on the defect-free and defect-containing surfaces of LiH crystal. Four substrate clusters are considered Li_2H_2, BeH_2, Li_8H_8 and $BeLi_6H_8$. These clusters were embedded in a three dimensional array of point charges and the point charges as well as the real ions were included in the Hamiltonian of the *ab initio* calculations. Figure 5 shows schematically the 3D unit cells and the path along which we have optimized the adatom - surface distance at selected locations Δ for BeH_2 and $BeLi_6H_8$ ion clusters.

The adsorption energy $E_{ads.}$ of the adatom on the substrate surface was calculated from the relation

$$E_{ads.} = E_{complex} - E_{adsorbate} - E_{substrate} \quad (1)$$

The terms appearing on the right hand side are the total energies of the complex (adsorbate + substrate), the adsorbate (free hydrogen atom) and the substrate (defect-free or defect- containing), obtained from three independent calculations using the same supercell. The negative adsorption energy $E_{ads.}$ indicates that the bound adsorbate is electronically stable.

The data for the selected substrate locations Δ along the diffusion path, equilibrium adsorbate - substrate distance R_e /Å and equilibrium adsorption energies E_{ads} / *eV* are collected in Table 3 and represented graphically in Figure 6. Defining the optimal adsorption site as the substrate location Δ at which the strongest adsorbate-substrate interaction occurs along the diffusion path, the optimal adsorption sites of the defect-free surfaces were found to be on the top of a substrate Li^+ ion, 4.5 Å above the substrate plane in Li_2H_2 and on the top of a substrate location Δ= 0.4, 3.8 Å above the substrate plane in Li_8H_8. The optimal adsorption sites of the defect-containing surfaces were found to be under the bottom of a substrate location Δ= 0.7, 0.035 Å under the substrate plane in BeH_2 and on the top of a substrate location Δ= 0.6, 0.55 Å above the substrate plane in $BeLi_6H_8$.

These results show that adsorption energies of atomic H have been enhanced by ca. 5.23 eV on Li_2H_2 cluster and by ca. 4.96 eV on Li_8H_8 after introducing the I-V dipole. A strong sign for interaction or chemical bond formation between adsorbate and substrate electronic states on the defect- containing surfaces is therefore expected, particularly in the vicinity

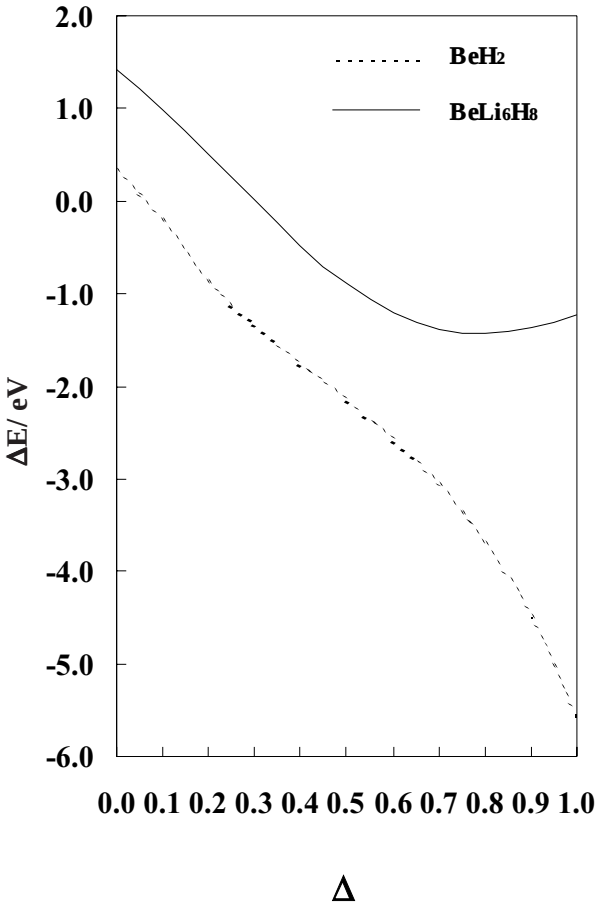

Figure 4 *Activation energy of $Be^{2+}V^-$ dipole migration in BeH_2 and $BeLi_6H_8$; Δ= 0.0 represents the (110) orientation, and Δ= 1.0 represents the (100) orientation*

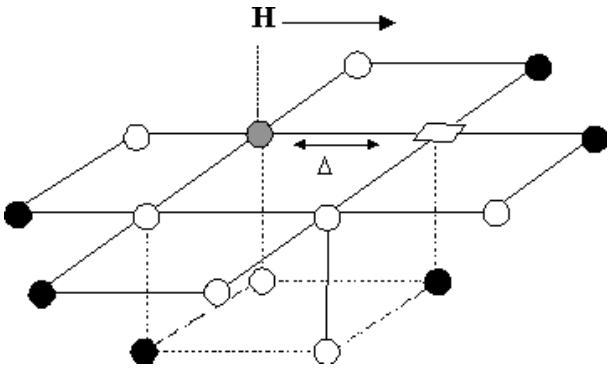

Figure 5 *Li_8H_8 and $BeLi_6H_8$ ion clusters and the path along which the adatom surface distance was optimized at selected locations Δ. ●: Be^{2+}, ○: H^-; ●: Li^+; □: vacancy*

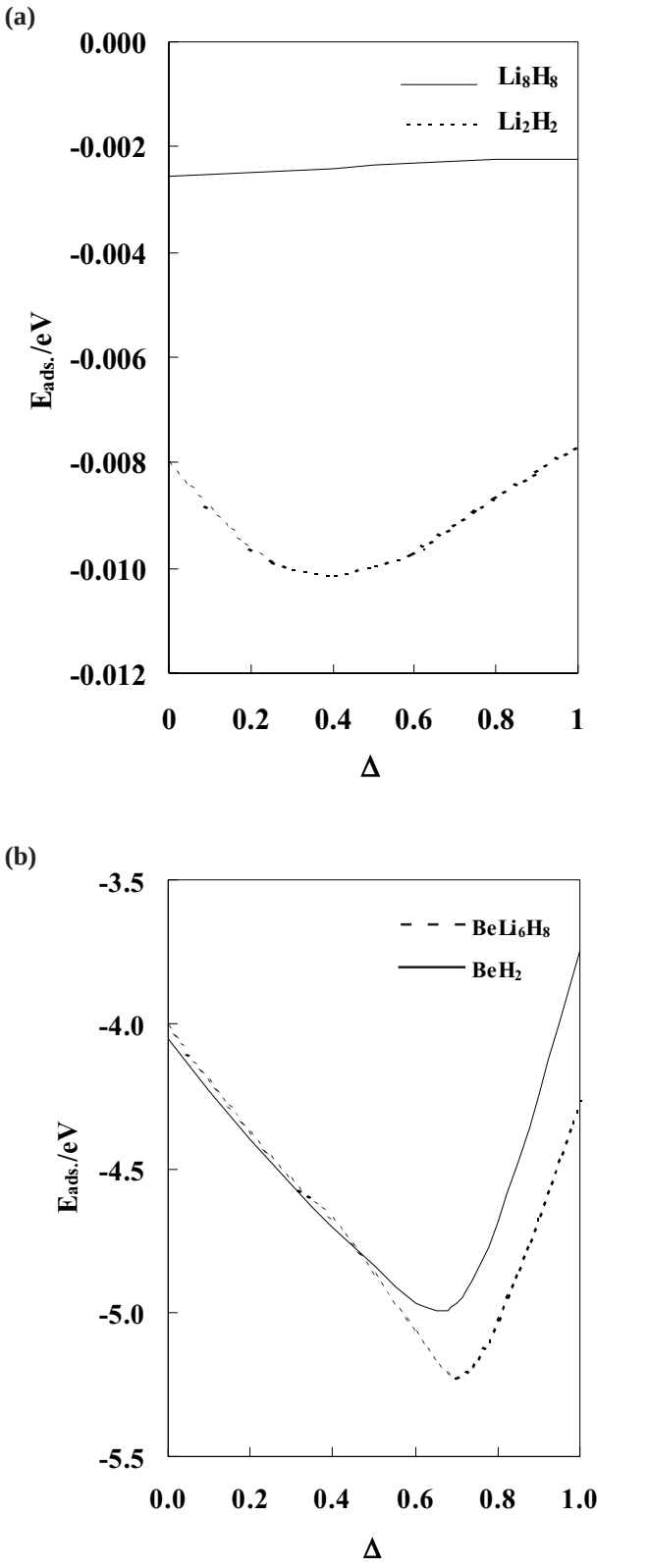

Figure 6 *Equilibrium adsorption energies E_{ads}. of atomic H on defect free (**a**, Li_2H_2 and Li_8H_8) and defect-containing (**b**, BeH_2 and $BeLi_6H_8$) surfaces of LiH crystal as a function in the substrate locations Δ = 0.00 → 1.00*

of the migrated cation vacancy, where the maximum increase of adsorption energie and decrease of adsorbate-substrate distance were observed. Moreover, the effect of increasing the size of the embedded cluster on adsorption energies and adsorbate-substrate distances was marginal implying that calculations carried out for small clusters might replace those for larger clusters so long as all clusters were embedded in the central region of the finite crystal surface, where the Coulomb field closely approximates that of the host surface.

Vidali et al. [18] reported 17.8 meV and 2.7 Å for adsorption energy and adsorbate-substrate distance in H/LiF (001) system. This may be compared with the present 10.1 meV and 3.8 Å for adsorption energy and adsorbate-substrate distance calculated for the adsorption of atomic H on the defect-free Li_8H_8 surface at the optimal substrate location Δ=0.4. The basic difference between adsorption energies and adsorbate-substrate distances in the two systems is attributed to the extended charge distribution of the hydride anion at LiH surface. Moreover, the present optimal substrate location Δ=0.4 is consistent with the role of steric hindrance and electronic repulsion between adsorbate and substrate electrons.

The electrostatic fields near the surface of an ionic crystal are large enough [19-21] that the polarization energy is a major component of the adsorption energy for many physisorped species. However, the fields are so nonuniform [22] that the dipole polarizability gives an inaccurate account of the polarization energy. Guo and Bruch [23] calculated the electrostatic polarization energy for H and He on LiF and MgO surfaces and reported that it contributes at the 10% level for atomic hydrogen. They also reported: ”The trend is that the electrostatic terms will be significant for more polarizable inert gases such as Kr and Xe”. Calculating the polarization energy to within 25% for such adsorbates will require inclusion of many multipole configurations

In Table 3 and Figure 6, binding of atomic H at Li^+ is strongly favored over binding at H^- of the Li_8H_8 defect-free surface, and binding at Be^{2+} is strongly favored over binding at the cation vacancy of the $BeLi_6H_8$ defect-containing surface, pointing to the probable diffusion of atomic H over the surface. To examine this probability, we have calculated the largest variations in adsorption energies and adsorbate-substrate distance. While the largest variation in the adsorption potential ca. 0.3 meV and in the adatom-surface distance ca. 0.1 Å occurs at a saddle point position on the top of the substrate Li^+ ion, 4.5Å above the substrate plane in Li_2H_2, the largest variation in the adsorption potential ca. 2.4 eV and in the adsorption height ca. 0.2 Å occurs at a saddle point position on the top of a substrate location Δ=0.4, 3.8 Å above the substrate plane in Li_8H_8. The diffusion barrier (or activation energy for diffusion) of the adsorbed H over the defect-free surface of LiH is therefore negligible and the mobility of the atomic H may not be considered as restricted. On the other hand, the largest variations in the adsorption potential ca. 1.22 eV and in the adsorbate-surface distance ca. 1.37 Å occurs at a saddle point position under the bottom of a substrate location Δ=0.7 under the substrate plane in BeH_2 and the largest variation in the adsorption potential ca. 0.92 eV and in the adsorbate-surface distance ca. 0.8 Å occur at a

saddle point position on the top of a substrate location Δ=0.6, 0.55 above the substrate plane in $BeLi_6H_8$. Here, the diffusion barriers of the adatom H over the defect- containing surfaces are quite significant and the mobility of adsorbed H over the surface is relatively restricted. We note, however, that in reality the adatom diffusion on this surface may include more complicated mechanisms, such as atomic exchange mechanisms, which we have not attempted to study here.

To investigate the differences in adsorption between the defect-free and defect-containing sites, the local densities of state (LDOS) have been evaluated for two-models, Li_8H_8 and $BeLi_6H_8$. In Li_8H_8 model, the band gap as the difference between HOMO (-9.75 eV) and LUMO (-1.67 eV), was calculated to be 8.08 eV. In $BeLi_6H_8$ model, the band gap as the difference between HOMO (-5.88 eV) and LUMO (-1.47 eV) was calculated to be 4.41 eV. The band gap was thus reduced by 3.67 eV as a consequence of the HOMO and LUMO shifting to higher energies. More specifically, the rise of HOMO level was much greater than the rise of the LUMO level. The energy levels of the hydrogen singly occupied and lowest unoccupied AO's were calculated to be -13.57 and 2.63 eV, respectively. The charge transfer occurs from the 1s AO to the surface unoccupied MO's (donation) and from the surface occupied MO's to the 1s singly occupied or lowest unoccupied A.O of H (back-donation). The charge transfer is therefore suggested to occur from the surface occupied MO's to the 1s singly occupied or lowest unoccupied AO of H (back-donation) in the course of adsorbate-substrate bond formation. The present cluster models do consider the Madelung potentials representing the ions in the rest of the crystal because they are regarded as a part of the solid. This implies that the calculated band gap narrowing is not exaggerated. Moreover, the calculated band gap narrowing, as a result of I-V dipole formation, shows that the electrical properties of LiH surface is significantly enhanced, even though it is still in the domain of insulating materials (≥ 2 eV). Since Hartree–Fock calculations often largely overestimate band gaps, DFT calculations were carried out for valance and conduction bands. DFT band gaps were calculated to be 7.9 and 4.26 eV for Li_8H_8 and $BeLi_6H_8$ surface clusters respectively. However, we have been unable to find experimental values of band gaps in LiH for comparison.

Summary and outlook

We have considered two possible orientations for $Be^{2+}V^{-}$ dipole at the surface of LiH crystal in addition to the effect of the I-V dipole formation on the nature of adsorbate-substrate interaction and diffusitivity of atomic H. The (100) orientation was found to be energetically more favorable than the (110) orientation. The (100) dipole changed the nature of atomic H adsortion from physisorption to chemisorption and the results were explained on basis of the differences in band gaps between adsorbate and substrate surfaces.

We have estimated the charges on the adsorbed hydrogen from the Mulliken method of population analysis and selected the optimal adsorption sites, Δ= 0.4 for Li_8H_8 defect- free surface and Δ= 0.6 for $BeLi_6H_8$ defect- containing surface. We expected a relationship between the charge on the adsorbate and the type of substrate surface. The charges on the H atom adsorbed at the defect- free and defect- containing surfaces were calculated to be 1.001 and 1.052 respectively. The larger charges assigned to the atomic H adsorbed at the defect-free and defect-containing surfaces - relative to the free H atom - imply that charge transfer takes place from the surface in consistence with the effect of I-V dipole on enhancing the adsorption, as well as the greater importance of surface HOMO's.

We have not attempted to study the relaxation of surface layer, but several calculations [24-26] show that properties of ions in the bulk of LiF and MgO are rather similar to the properties of the corresponding species near the surface and that the charge state [27] of the surface anions is nearly the same as in the bulk. Calculations give small relaxations of the surface layers, in agreement with low energy electron diffraction (LEED) experiments [28,29] but at variance with an ion channeling experiment [30]. The sensitivity of defect sites to cluster size and electrostatic environment may even be reduced by surface relaxation, though this remains a topic for future work.

References

1. Agullo-Lopez, F.; Catlow C.R.A; Townsend, P.D. *Point Defects in Materials;* Academic Press, Harcourt Brace Jovanovich Publishers: London 1988.
2. Bucci, G.; Fieschi, R. *Phys.Rev.Lett.* **1964**, *12*,16.
3. di Bartolo, B. *Optical Interactions in Solids*; Wiley: New York 1968.
4. Sugano, S.; Tanabe, Y.; Kamiura, H. *Multiplets of Transition Metal Ion in Crystals*; Academic Press: New York 1970.
5. Varostos, P.A.; Mourikis, S. *Phys.Rev.B* **1974**, *10*, 5220.
6. Ikeya, M. *J.Phys.Soc. Japan* **1977**, *42*, 168.
7. Kalman, K.; Toth, A.; Keszthelyi, T.; Sarkozi, J. *Mater.Sci.Eng*. **1982,** *54*, 85.
8. Toth, A.; Keszthelyi, T.; Kalman, P.; Sarkozi, J. *Mater.Sci.Eng.* **1984**, *64***,** 223.
9. Freund, H.J.; Umbach, E. *Adsorption on Ordered Surfaces of Ionic Solids and Thin Films;* Springer: Berlin, 1993.
10. Colbourn, E.A. *Reviews of Solid State Sciences* **1991**, *5*, 91.
11. Wimmer, E.; Fu, C.L.; Freeman, A.J. *Phys.Rev.Lett*. **1985**, *55,* 2618.
12. Mejias, J.A. *Phys.Rev.B.* **1996**, *53*, 10281.
13. Johnson, K.H.; Pepper, S.V. *J.Appl.Phys.* **1982**, *53*, 6634.
14. Anderson, A.B.; Ravimohan, C.; Mehandru, S.P. *Surf.Sci.* **1987**, *183*, 438.
15. Horsley, J.A. *J.Am.Cerm.Soc*. **1979**, *101*, 2870.

16. Shalabi, A.S.; El-Mahdy, A.M. *J.Phys. &Chem.Solids* **1999**, *60*, 305.
17. Gaussian 98, Revision A.6, Frisch, M.J.; Trucks, G.W.; Schlegel, H.B.; Scuseria, G.E.; Robb, M.A.; Cheeseman, J.R.; Zakrzewski, V.G.; Montgomery, J.A; Stratmann, Jr., R.E.; Burant, J.C.; Dapprich, S.; Millam, J.M.; Daniels, A.D.; Kudin, K.N.; Strain, M.C.; Farkas, O.; Tomasi, J.; Barone, V.; Cossi, M.; Cammi, R.; Mennucci, B.; Pomelli, C.; Adamo, C.; Clifford, S.; Ochterski, J.; Petersson, G.A.; Ayala, P.Y.; Cui, Q.; Morokuma, K.; Malick, D.K.; Rabuck, A.D.; Raghavachari, K.; Foresman, J.B.; Cioslowski, J.; Ortiz, J.V.; Stefanov, B.B.; Liu, G.; Liashenko, A.; Piskorz, P.; Komaromi, I.; Gomperts, R.; Martin, R.L.; Fox, D.J.; Keith, T.; Al-Laham, M.A.; Peng, C.Y.; Nanayakkara, A.; Gonzalez, C.; Challacombe, M.; Gill, P.M.W.; Johnson, B.; Chen, W.; Wong, M.W.; Andres, J.L.; Gonzalez, C.; Head-Gordon, M.; Replogle, E.S.; Pople, J.A., Gaussian, Inc., Pittsburgh PA, 1998.
18. Vidali, G.; Ihim, G.; Kim H.-Y.; Cole, M.W. *Surf.Sci.Rep.* **1991**, *12*,133.
19. (a) Gready , J.E.; Bacskay , G.B.; Hush, N.S. *J.Chem.Soc.Faraday Trans.II* **1978**, *74*,1430; (b) Dovesi, R.; Orlando, R.; Ricca F.; Roetti, C. *Surf.Sci.* **1987**, *186*, 267.
20. (a) Deprick B.; Julg, A. *Nouv.J.Chem*. **1987**, *11*,299; (b) Deprick B.; Julg, A. *Chem.Phys.Lett.* **1984**, *110*, 150.
21. (a) Lakhlifi A.; Girardet, C. *J.Chem.Phys.* **1991**, *94*, 688; (b) Lakhlifi A.; Girardet, C. *Surf.Sci.* **1991**, *241*, 400; (c) Girardet, C.; Girard, C. *Surf.Sci*. **1988**, *201, 278;* (d) Girardet, C.; Girard, C. *Chem.Phys.Lett.* **1987**, *138*, 83; (e) Girard, C.; Mghezzi, C.; Vigoureux, J.M. *Chem.Phys.* **1989**, *136*, 47.
22. (a) Lennard-Jones, J.E.; Dent, J.E. *Trans. Faraday Soc.* **1928**, *24*, 92; (b) Nijboer, B.R.A. *Physica* **1984**, *125A*, 275.
23. Guo, Z.-C.; Bruch, L.W. *J.Chem.Phys*. **1992**, *97*, 7748.
24. Fowler, P.W.; Hutson, J.M. *Phys.Rev.B* **1986**, *33*, 3724.
25. Fowler, P.W.; Tole, P. *Surf.Sci*. **1988**, *197*, 457.
26. Causa, M.; Dovesi, R.; Pisani, C.; Roetti, C. *Surf.Sci.* **1986**, *175*, 551.
27. Causa, M.; Dovesi, R.; Pisani, C.; Roetti, C. *Acta Crystal. B* **1986**, *42*, 247.
28. (a) Kinniburgh, C.G. *J.Phys.* **1976**, *C9***,** 2695; (b) Welton-Cook M.R.; andBernardi, W. *J.Phys.* **1982**, *15*, 569; (c) Urano, T; Kanaji T.; Kaburagi, M. *Surf.Sci.* **1983**, *134*,109; (d) Maksym, P.A. *Surf.Sci.* **1985**, *149*, 157.
29. (a) Blanchard, D.L.; Lessor, D.L.; La Femina, P.J.; Baer, D.R.; Ford, W.K.; Guo, T. *J.Vac.Sci.Technol*. **1991**, *A9*, 1814; (b) Jung, D.R.; Cui, J.; Frankl, D.R. *J.Vac.Sci.Technol*. **1991**, *9*,1589.
30. (a) Nakamatsu, H.; Sudo, A.; Kawai, S. *Surf.Sci.* **1988**, *194*, 265; (b) see also: DeCrescenzi, M.; Motta, N.; Patella, F.; Sgarlata, A.; Arciprete, F.; Balzarotti, A.;Benfatto, M.; R.Natoli, C.R. In *The Structure of Surfaces III*; Tong, S.Y.; van Hove, M.A.; Takayanagi, K.; Xie X.D., Eds.; Springer: Berlin, 1991; p 665.